Theory of the phase diagram of iron and thallium: The Burgers and Bain deformation mechanisms revised

V. P. Dmitriev and Yu. M. Gufan
Institute of Physics, Rostov State University, 344104 Rostov on Don, U.S.S.R.

P. Tolédano
Laboratory of Phase Transitions, University of Amiens, 80000 Amiens, France
(Received 10 October 1990)

A theoretical model is proposed for the pressure-temperature phase diagram of iron and thallium. A unified phenomenological and atomistic description is given for the Burgers and Bain deformation mechanisms. The bcc-hcp and bcc-fcc transformations are associated, respectively, with six- and two-dimensional order parameters, which are expressed as periodic functions of the atomic displacements. The fcc-hcp transformation is interpreted as a displacive transition between two low-symmetry phases. A thermodynamic potential describing the three preceding transformations is constructed, and the corresponding theoretical phase diagram, including the triple point, is worked out. It is compared to the experimental phase diagrams of iron and thallium.

I. INTRODUCTION

In a series of recent papers,[1-5] a theory of reconstructive transitions was developed by the authors of this work, in which two main classes of transitions were distinguished: (1) Transitions for which the mechanism can be formulated in terms of atomic displacements. For this category of transitions it was shown[1-3] that the order parameter can be expressed as a transcendental function of the average displacements which occur at the transitions. As standard examples, the bcc-to-hcp and bcc-to-fcc transformations were considered. (2) The martensitic fcc-to-hcp transformation for which it was shown[4,5] that the two phases could be interpreted as the result of ordering mechanisms from a disordered latent parent structure formed by hexagonal polytypes.

In crystals of the elements Ba, Tl, Fe, and Yb,[6] the three (fcc, bcc, and hcp) phases are found to coexist and to merge at a triple point. In such a situation, it is of interest to determine which of the mechanisms — displacive or reordering — dominates and how they coexist in the vicinity of the triple point. The aim of this paper is to present a comprehensive description of the corresponding phase diagrams and to show that the fcc and hcp phases can actually be obtained from independent displacive mechanisms from the common parent bcc structure, whereas no reordering mechanism takes place in this case at the fcc-to-hcp transformation.

The paper is organized as follows. As a preliminary section, a unified phenomenological and atomistic description is given (Sec. II) of the two classical mechanisms, i.e., the Burgers mechanism[7] and the Bain deformation,[8] which are currently associated with the bcc-hcp and bcc-fcc transformations. The theoretical phase diagram, which includes the three distinct phases, is then worked out (Sec. III) and compared to the experimental pressure-temperature phase diagrams which are available for iron[9] and thallium[10] (Sec. IV). The experimental data concerning Ba and Yb will not be discussed because only narrow regions of their phase diagram are known with accuracy.

II. UNIFIED DESCRIPTION OF THE BURGERS MECHANISM AND BAIN DEFORMATION

A. Burgers mechanism reformulated

The mechanism generally assumed for the bcc-to-hcp transformation is the so-called Burgers mechanism.[7] It can be divided into three stages [Figs. 1(a) and 1(b)]. In the first stage the (110) bcc planes transform into the (001) hcp planes. Second, a homogeneous shifting of the atoms in the (110) bcc planes leads to a virtual fcc structure. Third, the displacement of one out of two planes in the [110] bcc direction leads to the formation of the hcp structure. Accordingly, Burgers' mechanism involves three different and simultaneous instabilities associated with distinct primary (symmetry-breaking) order parameters.

In contrast to the preceding scheme, we propose a transition mechanism based on a *single* primary order parameter, which consists in an antiparallel shifting of the atoms lying in the (110) bcc planes along the $[\bar{1}10]$ and $[1\bar{1}0]$ bcc directions [Fig. 1(c)]. It induces, as a secondary effect, a compression of the cubic unit cell along one of the fourfold axis [001], and a simultaneous decompression along the two other ([100] and [010]), fourfold axes. A more concrete view of the assumed mechanism at the atomistic level is shown in Fig. 2. Each (110) bcc layer is organized in such a manner that, in any triangle formed by neighboring atoms, two sides are formed by atoms which touch each other, and the third side is formed by separated atoms [Figs. 2(a) and 2(b)]. It is on the third

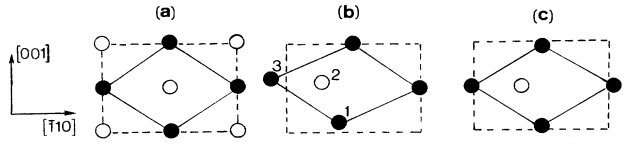

FIG. 1. Projection of the bcc and hcp unit cells on the (110) bcc plane. Solid and open atoms are, respectively, in positions $\frac{1}{2}$ and 0. (a) Initial bcc structure. (b) hcp structure following Burgers mechanism: the atoms denoted 1, 2, 3 are shifted along the same $[1\bar{1}2]_{bcc}$ direction. (c) hcp structure following our mechanism: the displacements are along the $[1\bar{1}0]_{bcc}$ direction. The deformation along $[001]_{bcc}$ is induced by the shifting of the open sublattice.

side that the atoms of the next layer are located. The displacement of one layer with respect to the following one in the [110] bcc direction (i.e., the shifting of each atom of the upper layer towards the center of the corresponding triangle, which is formed by the atoms of the lower layer) allows the separated atoms to come in contact, and thus to form a regular double-layered hexagonal-close-packed structure. The reverse sliding of one close-packed layer with respect to the next layer, at fixed interlayer distance, breaks one of each of the three pairs of atoms touching each other, again forming a bcc lattice.

In the formalism of group theory, the primary order parameter in our mechanism transforms as the irreducible representation (IR) denoted $\tau_4(k_9)$ in the Kovalev notation,[11] which is a six-dimensional IR of the O_h^9 ($Im3m$) space group, at the N point of the bcc Brillouin zone [$k_9=(\frac{1}{2},\frac{1}{2},0)$]. The secondary order parameter (the deformation) has the symmetry of the two-dimensional IR of the O_h^9 group at the Γ point ($k=0$), which is spanned by the two combinations of strain-tensor components:[12]

$$\eta_1=\frac{1}{\sqrt{6}}(e_{xx}+e_{yy}-2e_{zz})$$

and (1)

$$\eta_2=\frac{1}{\sqrt{2}}(e_{xx}-e_{yy})\ .$$

In other words, the bcc-to-hcp transformation is interpreted as an improper ferroelastic transition.[12] The improper character of the spontaneous strain is attested experimentally by the fact that, in crystals of the elements,[6,13] the distance between the atomic layers parallel to $(110)_{bcc}$ or $(001)_{hcp}$ remains practically unchanged from the bcc to the hcp phase.

Let us now emphasize that the hcp phase *is not* a ferroelastic phase in the usual sense, as its space group [D_{6h}^4 ($P6_3/mmc$), $Z=2$] corresponds actually to an *enlargement* of the ferroelastic group D_{2h}^{17} ($Cmcm$, $Z=2$) induced by the IR $\tau_4(k_9)$. The mechanism of the enlargement of the orthorhombic to a hexagonal symmetry is represented in Figs. 3(a) and 3(b). One can see that, for a general shifting of the atoms along the $[1\bar{1}0]$ bcc direction, the O_h^9 symmetry is lowered to D_{2h}^{17}, but for the specific shifting $a\sqrt{2}/12$, where a is the cubic lattice parameter, the symmetry *increases* to D_{6h}^4. In projection in the $(1\bar{1}0)$ bcc plane, one can verify that, after such a large

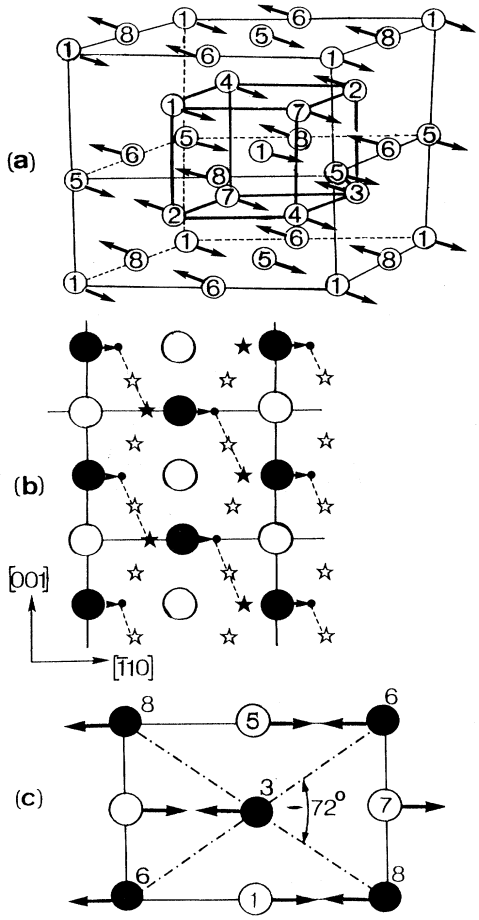

FIG. 3. Average shifting of the atoms from the bcc to the hcp structure. The displacements are symbolized by arrows. Solid and open circles represent atoms located in two adjacent layers. (a) The small cube (thick lines) is the bcc unit cell. The large cube is an extended unit cell obtained when all the branches of $\mathbf{k}_9^*$ are active. (b) Projection on the (110) bcc plane. The shifting from the bcc (large circles) to the hcp structure (small circles) is $a\sqrt{2}/12$. The open and solid stars correspond to virtual positions at which the symmetry would increase respectively to O_h^9 and D_{6h}^4. (c) Projection on the $(1\bar{1}0)$ bcc plane. After the shifting, the angle between the diagonals becomes 60°.

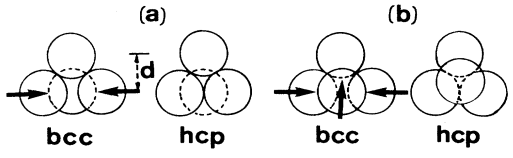

FIG. 2. Atomic model illustrating the improper character of the macroscopic deformation, induced by the atomic displacements represented by arrows. (a) Projections of the bcc and hcp structures, respectively, on the (001) bcc and $(\bar{1}10)$ hcp planes. d is the interatomic distance. (b) Projections of the bcc and hcp structures, respectively, on the (110) bcc and (001) hcp planes.

shift, the angle between the threefold axes, which is about 72° in the cubic cell, becomes 60° in the hexagonal cell [Fig. 3(c)].

A striking property, which can be foreseen from Fig. 3(b), is the *periodic* connection that can be found between the overall symmetry undertaken by the crystal and the virtual displacements of the atoms along the [110] cubic direction. Thus, for general displacements along [110], the system exhibits the symmetry D_{2h}^{17}, while for the specific displacements $a\sqrt{2}/12$, $7a\sqrt{2}/12$, ..., the system regains the D_{6h}^{4} hcp symmetry. For other specific displacements, namely $a\sqrt{2}/4, 3a\sqrt{2}/4, \ldots$, the symmetry increases to D_{6h}^{1} (**P6/mmm**, $Z=1$). These considerations allow us to define the order-parameter modulus ζ in the function of the average displacements ξ as

$$\zeta=\zeta_0\left[\sin\left[\frac{4\pi\xi}{a}+\frac{\pi}{2}\right]-\frac{1}{2}\right] . \tag{2}$$

The form of the preceding function is justified in Fig. 4(a), which shows that, for successive values of ξ along [110], one periodically gets the sequence of the O_h^9, D_{2h}^{17}, D_{6h}^{4}, and D_{6h}^{1} phases. However, Eq. (2) has been obtained by considering the atoms as located at points of the lattice and this leads, for the phase of D_{6h}^{1} symmetry, to a configuration in which the atoms of one layer are exactly over the atoms of the next layer, i.e., a situation which implies a considerable increase of the interlayer distance or a noticeable deformation of the atoms. As neither happen in the close-packed hard-sphere model under consideration, one has to introduce the geometrical constraints imposed by the size of the atoms. In particular, one can see in Fig. 3(b) that the realistic path followed by the atoms after reaching the hcp structure, is to be shifted along the directions $[120]_{hcp}$, $[210]_{hcp}$, or $[110]_{hcp}$, i.e., to pass through valleys between touching atoms. This excludes the phase of symmetry D_{6h}^{1} to be formed and yields a simplified dependence of the order- parameter modulus in function of the displacements:

$$\zeta=\zeta_0\sin(6\pi\xi/a\sqrt{2}) . \tag{3}$$

Equation (3) is represented in Fig. 4(b). It corresponds to a more physically realistic scheme; one can see, in particular, that the condition imposed to the order parameter, i.e., to be equal to zero in the parent phase, is fulfilled by Eq. (3) and not by Eq. (2).

B. Bain deformation revised

Let us now focus on the bcc-to-fcc transformation. One can visualize the way a bcc lattice transforms into a fcc lattice via a deformation which stretches the cubic unit cell along one of the fourfold axes (e.g., [001]) and compresses it by the same extent along the two other fourfold axes. Such a deformation is called the Bain deformation.[8] The spontaneous strain-tensor components which express this deformation are given by Eq. (1), i.e., from the basis of the same two-dimensional zone-center IR of the O_h^9 space group that has been considered in Burgers mechanism. A tetragonal structure [space group D_{4h}^{17} ($I4/mmm$), $Z=1$] is obtained for the following equilibrium values of the corresponding order parameter:[12] $\eta_1=\eta\neq 0$, $\eta_2=0$. However, when the deformation coincides with the specific ratio $c/a=\sqrt{2}$ (a and c being the lattice parameters of the tetragonal unit cell), the tetragonal structure identifies as a face-centered-cubic structure (space group O_h^5) as represented in Figs. 5(a) and 5(b).

As the bcc-to-hcp transformation, the Bain deformation has a periodic character which can be seen by considering the angle ϕ between the diagonals of the (110) cubic plane (Fig. 6). Thus, in the bcc lattice, $\phi=\arccos\frac{1}{3}\simeq 70°32'$. For $\phi=90°$, the (110) bcc planes transform into the (010) fcc planes and the space group of the crystal becomes O_h^5 ($Fm3m$). Further increase of the

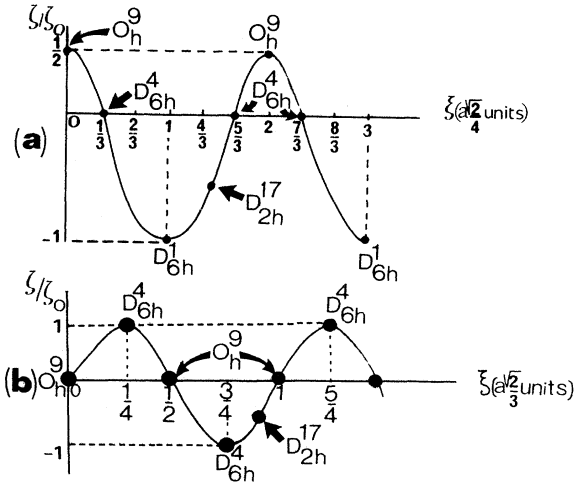

FIG. 4. Periodic dependence of the order parameter for the bcc-hcp transformation following (a) Eq. (2) and (b) Eq. (3).

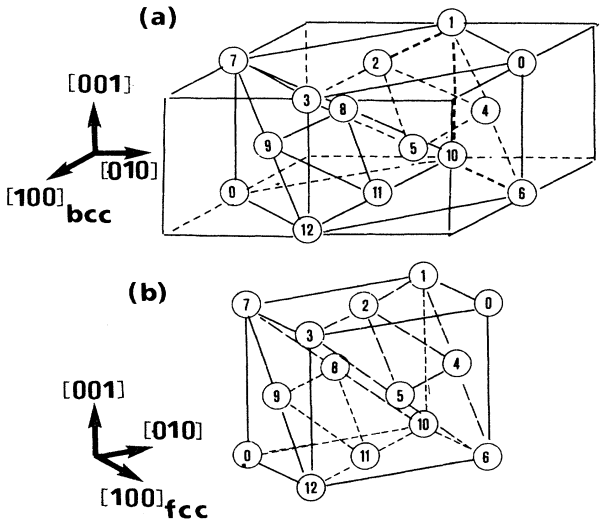

FIG. 5. Unit cells corresponding to the (a) bcc and (b) fcc structures.

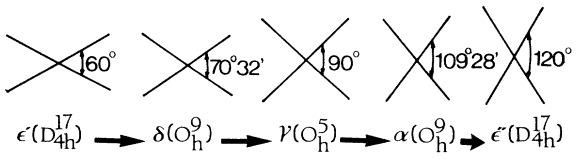

FIG. 6. Periodic character of the bcc-fcc Bain deformation of the iron unit cell, viewed by our considering the angle between the diagonals in the (110) cubic plane.

angle ϕ up to $\phi=109°28'$ brings about the crystal again to the bcc (O_h^9) symmetry, but with a different orientation with respect to the initial bcc structure. Besides, for the values $\phi=60°$ and 120°, one obtains a hexagonal lattice, which prefigures the hcp phase (Fig. 6). The dependence of the order-parameter modulus in function of the angle can be written here:

$$\eta=\eta_0\left[\sin\left[6\phi-\frac{\pi}{2}\right]-\cos(6\arccos\tfrac{1}{2})\right]. \tag{4}$$

The variation of the function $\eta(\phi)$ is shown in Fig. 7(a). One can notice that, in contrast to Eqs. (2) and (3), the variation law represented by Eq. (4) does not hold for any value of ϕ, as ϕ represents an *absolute* measure of the angle between the diagonals and is thus restricted by the following constraints: (1) The argument of $\eta(\phi)$ should be limited as it expresses the macroscopic deformation of a crystal. (2) After reaching the value $\phi=90°$, a close-packed fcc structure is formed and a further deformation of the unit cell along the $[100]_{bcc}\|[110]_{fcc}$ directions is impossible, at least if one assumes a hard-sphere model; as in the preceding directions, close-packed chains of atoms are formed with atoms in contact with each other.

In order to remove the preceding restrictions, one

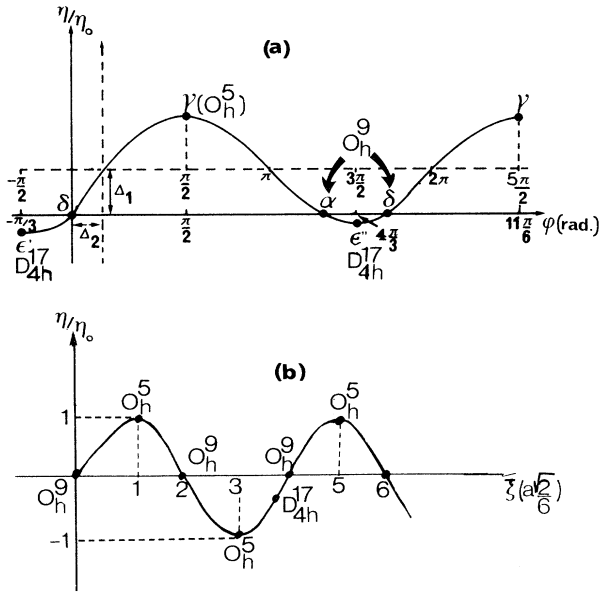

FIG. 7. Periodic dependence of the order parameter for the bcc-fcc transformation following (a) Eq. (4) and (b) Eq. (5).

should express the order parameter as a function of the average displacements of the atoms. This brings us to analyze the atomistic mechanism which underlies the Bain deformation, inspiring ourselves from the shearing deformation model currently proposed for the bcc-to-fcc transformation.[14] According to this model, the structural stability of the bcc structure is lowered with respect to an homogeneous shear strain of the (011) planes in the [011] directions, which gives rise to a fcc structure. An experimental support to this interpretation is the decrease of the shear modulus C_{11}-C_{12} observed in a number of bcc metals when approaching the fcc phase. In reference to Figs. 5(a) and 5(b), we can propose the following path which materializes the preceding macroscopic mechanism at the atomistic level: (1) the layer containing the atoms labeled 7–12 is shifted by $a\sqrt{2}/6$ in the [011] bcc direction, the atom in 0 position reaching the center of a triangle formed by the atoms denoted 8, 9, and 11; (2) the next layer, formed by atoms 1–6 will be subsequently shifted by $a\sqrt{2}/3$ (this will place each atom initially in 0 position, at the center of the corresponding triangles of the following layer); (3) at last, a shifting of the third layer by $a\sqrt{2}/2$ will force the atoms located in this layer to occupy equivalent positions, i.e., the corner atoms (0,0) will lie on a straight line passing by the centers of the triangles 8, 9, 11, and 2, 4, 5 and orthogonal to the three successive layers. Hence, the layers containing the atoms labeled 0 in Figs. 5(a) and 5(b) will be equivalent crystallographically, i.e., the resulting structure will consist of a three-layered close-packed structure (a fcc structure) since the shears will have eliminated the repulsive effect of one layer with respect to the neighboring ones.

Let us stress that the hereabove mechanism proposed for the Bain deformation is closely analogous to the Burgers mechanism, as both mechanisms preserve the interlayer distance and thus the repulsive effect of one layer with respect to the others. The essential difference is that, in the bcc-to-hcp transformation, two successive layers are assumed to shift in opposite directions, i.e., the displacements are associated with a soft mode at the surface of the bcc Brillouin zone, whereas for the bcc-to-fcc transformation, two successive layers are sheared in the same direction, and thus correspond to a zone-center soft mode.

In agreement with the atomistic mechanism introduced for the Bain deformation, one can rewrite the dependence of the order parameter η as a function of the displacements ξ along the [011] direction as

$$\eta=\eta_0\sin(3\pi\xi/a\sqrt{2}). \tag{5}$$

Equation (5) is represented in Fig. 7(b). The function (5) is, in contrast to the definition given by Eq. (4), now valid for *infinite* displacements, at least when taking into account the cyclic conditions related to the periodic character of the lattice.

III. THEORETICAL PHASE DIAGRAM

Let us now deal with the thermodynamic description of the Burgers mechanism and Bain deformation. We will first work out the diagram associated with each one

of these two transformations, then the situation in which the two mechanisms are coupled, i.e., where the three phases have regions of coexistence, will be considered.

According to Sec. II, the order parameter (ξ_i) associated with the bcc-to-hcp transition transforms as the six-dimensional IR $\tau_4(k_9)$ of the O_h^9 space group. Using the results of Ref. 12, one has the corresponding order-parameter expansion:

$$F_1(\xi_i)=F_{10}+\frac{\alpha}{2}J_1+\frac{\beta_1}{4}J_1^2+\frac{\beta_2}{2}J_2+\frac{\beta_3}{2}J_3+\beta_4 J_4 +\gamma_1 J_1^3+\gamma_2 J_1 J_2+\gamma_3 J_1 J_3+\gamma_4 J_1 J_4 , \quad (6)$$

where

$$J_1=\sum_{i=1}^{6}\xi_i^2,$$

$$J_2=\xi_1^2\xi_2^2+\xi_3^2\xi_4^2+\xi_5^2\xi_6^2,$$

$$J_3=\sum_{i\neq j}\xi_i^2\xi_j^2-J_2,$$

and

$$J_4=\xi_i\xi_2\xi_3\xi_4+\xi_1\xi_2\xi_5\xi_6+\xi_3\xi_4\xi_5\xi_6 .$$

Expansion (6) has been restricted to the sixth degree, which is the lowest degree required by the first-order character of the bcc-to-hcp transition. The equilibrium condition realized for the stabilization of the phase of orthorhombic symmetry D_{2h}^{17} is[12]

$$\zeta_1=\zeta\neq 0, \quad \zeta_2=\ldots=\zeta_6=0 . \quad (7)$$

The introduction of (7) in (6) yields the *effective* thermodynamic potential for the bcc-to-hcp transition:

$$F_1(\zeta)=F_{10}+\frac{a_1}{2}\zeta^2+\frac{a_2}{4}\zeta^4+\frac{a_3}{6}\zeta^6 , \quad (8)$$

where ζ is given by Eq. (3). The equation of state obtained by a minimization of F_1 with respect to the displacements ξ is

$$\frac{\partial F_1}{\partial \xi}=\zeta(a_1+a_2\zeta^2+a_3\zeta^4)\frac{\partial \zeta}{\partial \xi}=0 . \quad (9)$$

It leads to the three possible stable states which have been visualized in Fig. 4(b), namely: (1) Two differently oriented domains of the bcc phases for $\zeta=0$. The two domains correspond to the respective sets of displacements along [110]: $\xi=0, a_3\sqrt{2}/3, 2a\sqrt{2}/3, \ldots$, and $\xi=a\sqrt{2}/6, 5a\sqrt{2}/6, 9a\sqrt{2}/6, \ldots$, and can be deduced one from another by a rotation of 90°around [110]. (2) Two analogous domains of the hcp structure for $\partial\zeta/\partial\xi=0$, i.e., for $\xi=a\sqrt{2}/12, 5a\sqrt{2}/12, 9a\sqrt{2}/12, \ldots$, or $\xi=3a\sqrt{2}/12, 7a\sqrt{2}/12, \ldots$. (3) two domains of orthorhombic symmetry D_{2h}^{17} for

$$\zeta^2=\frac{a_2+(a_2^2-4a_1a_3)^{1/2}}{2a_3}$$

corresponding to general displacements along [110].

Following the denomination used in Ref. 1, the hcp structure is a *non-Landau phase,* i.e., a phase which is stabilized only because a periodic nonlinear dependence of the order parameter as a function of the displacements is taken into account. The order parameter has a constant value *below* the transition, as it corresponds to specific fixed displacements. This is in contrast with the *Landau phase* of symmetry D_{2h}^{17}, which has a standard temperature- dependent variation below the transition.

The phase diagram associated with the potential $F_1(\zeta)$ is represented in Fig. 8(a) in the plane of the phenomenological coefficients (a_1,a_2). One can see that the bcc and hcp phases are separated by a line of first-order transitions which is bounded by two limits of stability lines in which the two phases coexist. The orthorhombic phase is separated from the hcp phase by a line of second-order transitions and can be reached from the bcc phase either across a second-order transition line ($a_1=0$) or through a line of first-order transitions (ON). Point O is a tricritical point. In order to have a line of first-order transitions between the hcp and D_{2h}^{17} phases, $F_1(\zeta)$ should be expanded up to the eighth degree. Figure 8(a) illustrates a general property of phase diagrams containing Landau and non-Landau phases, that has been established in Ref. 2, namely, that the boundary of non-Landau phases are hyperplanes in the n-dimensional space of the phenomenologi-

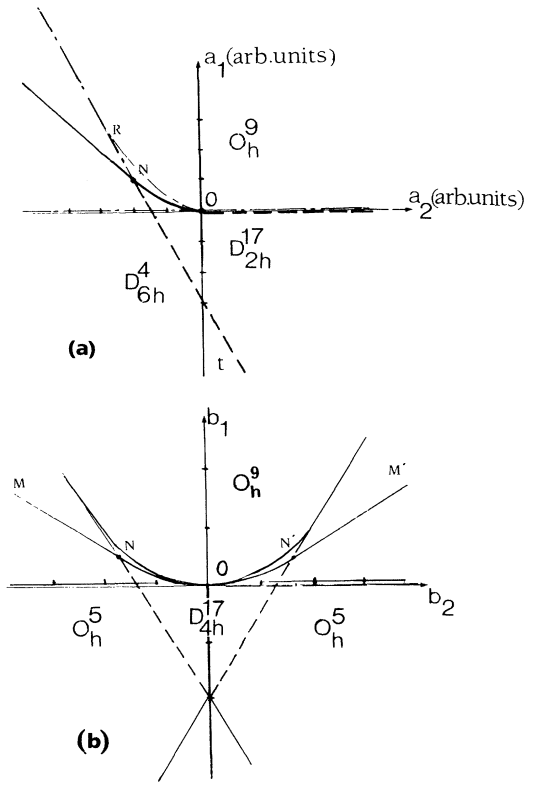

FIG. 8. Phase diagrams obtained by minimization of the thermodynamic potential (8) for the (a) bcc-hcp transformation and of potential (10) for the (b) bcc-fcc transformation. Solid, dashed, and dash-dotted lines are, respectively, first-order, second-order transition lines, and limit of stability lines.

cal coefficients, i.e., a straight line in the present case with $n=2$, and that the hyperplanes are tangent to the boundary of stability of the Landau phases (here at point R).

The bcc-to-fcc transition is associated with the two-component order parameter given by Eq. (1). From the corresponding IR at the center of the bcc Brillouin zone, one can construct the following order-parameter expansion:

$$F_2(\eta_1,\eta_2)=F_{20}+\frac{\alpha}{2}(\eta_1^2+\eta_2^2)+B(\eta_1^3-3\eta_1\eta_2^2)+\frac{\beta_1}{4}(\eta_1^4+\eta_2^4)+\frac{\beta_2}{2}\eta_1^2\eta_2^2 , \quad (10)$$

which contains a cubic invariant. The equilibrium condition realized in the tetragonal phase of symmetry D_{4h}^{17} is[12]

$$\eta_1=\eta\neq 0, \quad \eta_2=0 , \quad (11)$$

so that the effective thermodynamic potential associated with the bcc-fcc transition takes the simplified form

$$F_2(\eta)=F_{20}+\frac{b_1}{2}\eta^2+\frac{b_2}{3}\eta^3+\frac{b_3}{4}\eta 4 , \quad (12)$$

where the dependence of η as a function of the displacements ξ is given by Eq. (5). The equation of state is

$$\eta(b_1+b_2\eta+b_3\eta^2)\frac{\partial\eta}{\partial\xi}=0 , \quad (13)$$

which again provides three possible stable states: (1) the bcc phase for $\eta=0$, with two differently oriented domains associated with the respective displacements $(\xi=0,2a\sqrt{2}/3,\ldots)$ and $(\xi=a\sqrt{2}/4,a\sqrt{2},\ldots)$; (2) the fcc "non-Landau" phase for $\partial\eta/\partial\xi=0$ with two domains turned one with respect to the other by 90° around the cubic axis [110] and corresponding, respectively, to the shifts $(a\sqrt{2}/6,5a\sqrt{2}/6,\ldots)$ and $(a\sqrt{2}/2,7a\sqrt{2}/6)$; and (3) the tetragonal phase of symmetry D_{4h}^{17} for

$$\eta^2=\frac{-b_2+(b_2^2-4b_1b_3)^{1/2}}{2b_3} ,$$

which takes place for a general (nonspecific) displacement.

The phase diagram corresponding to the potential $F_2(\eta)$ is given in Fig. 8(b). One can verify that the two differently oriented fcc domains are separated from the parent bcc phase by straight lines of first-order transitions (NM and $N'M'$), which are tangent at $(b_1=0,\ b_2=0)$ to the second-order transition line which limits the bcc and tetragonal phases. These latter phases can be reached from the fcc phase across a line of second-order transition.

In order to investigate the region at which the three (bcc, hcp, and fcc) phases merge, one should use the thermodynamic potential:

$$F(\zeta,\eta)=F_1(\zeta)+F_2(\eta)+F_3(\zeta,\eta) , \quad (14)$$

where $F_3(\zeta,\eta)$ is the coupling free energy between the order-parameters ζ and η. Following a standard procedure,[15] the lowest-degree coupling terms are found to be

$$F_3(\zeta,\eta)=\delta\eta\zeta^2+\frac{\gamma}{2}\eta^2\zeta^2 . \quad (15)$$

Denoting ξ_1 and ξ_2 the independent displacements associated, respectively, with the bcc-hcp and bcc-fcc transformations, minimization of $F(\zeta,\eta)$ with respect to ξ_1 and ξ_2 yields the equations of state

$$\zeta(a_1+a_2\zeta^2+a_3\zeta^4+2\delta\eta\zeta+\gamma\eta^2)\frac{\partial\zeta}{\partial\xi_1}=0 , \quad (16)$$

$$(b_1\eta+b_2\eta^2+b_3\eta^3+\delta\zeta^2+\gamma\eta\zeta^2)\frac{\partial\eta}{\partial\xi_2}=0 . \quad (17)$$

Restricting the discussion of Eqs. (16) and (17) to the region in which the three phases are close to the triple point, one obtains the phase diagram of Fig. 9. A more striking feature of this diagram, which contains the two non-Landau hcp and fcc phases, is that all the transitions and limits of the stability lines are straight lines. Thus, the equations corresponding to the lines of first-order transitions are $a_1+a_2+a_3=0$ (bcc-hcp), $b_1+b_2+b_3=0$ (bcc-fcc), and $a_1+a_2+a_3=b_1+b_2+b_3\neq 0$ (fcc-hcp). The preceding lines intersect at the triple point T, whose coordinates are in the (a_1,b_1) plane: $(-a_2-a_3,\ -b_2-b_3)$. The equations corresponding to the limit of stability lines are $a_1=-\gamma-\delta$ (for the bcc into the hcp phase), $b_1=-(3b_2+b_3)$ (for the fcc into the bcc phase), $b_1=-\gamma$ (for the bcc into the fcc phase) and $a_1=-(2a_2+a_3)$ (for the hcp into the bcc phase).

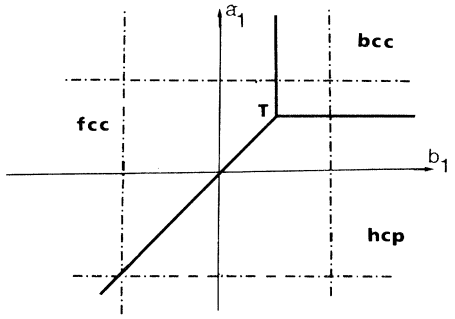

FIG. 9. Phase diagram associated with the potential (14) in the region of the triple point. Solid and dash-dotted lines are first-order transition and limit of stability lines.

IV. DISCUSSION AND CONCLUSION

The pressure-temperature phase diagram of iron[9] is schematized in Fig. 10(a). At atmospheric pressure, iron crystallizes from the melt into the bcc structure (δ-Fe) and at lower temperature transforms into the austenite fcc phase (γ-Fe) and again into a bcc structure (α-Fe). With increasing pressure, a triple point is found[9] at $P_t\simeq 97$ kbar and $T_t\simeq 450$ °C, at which the γ and α phases merge with the hcp ε phase. The diagram of Fig. 10(a) illustrates the following features of our model

(1) The δ and α bcc phases can be interpreted as the

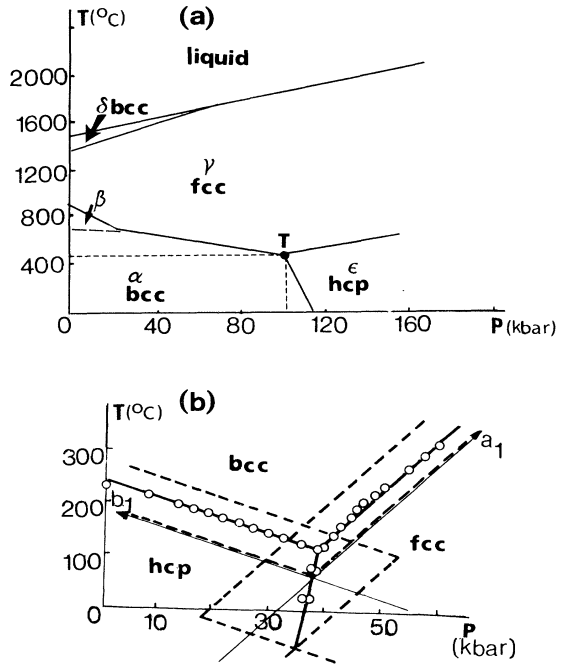

FIG. 10. (a) Schematic representation of the phase diagram of iron from Ref. 9. The β phase has a bcc structure and differs from the α structure only by its magnetic ordering. (b) superposition of the experimental points, given by Jajaraman *et al.* (Ref. 10) for the phase diagram of thallium and of the best fit deduced from the theoretical diagram of Fig. 9, after a linear tranformation of the (a_1,b_1) plane into the pressure-temperature plane.

two differently oriented structures predicted from the periodic dependence of the order parameter, as represented in Fig. 6. No available data allows one to compare the different orientations assumed in our model for the δ and α structures. A diffraction spectrum of the two phases should provide such a verification since cycling across the transition should progressively lead to a replacement of twofold positions (e.g., in the cubic direction [110]) by a fourfold diffraction pattern.

(2) The virtual pseudohexagonal tetragonal phases, denoted ε' and ε'' in Fig. 6 (i.e., a tetragonal lattice with 60° angles between the diagonals), prefigure the formation of the hcp ε phase, as the D_{4h}^{17} symmetry of the ε' and ε'' phases was shown in Sec. II to transform into D_{6h}^{4} for specific displacements.

(3) The metastable regions of the bcc phase into the fcc and hcp phases, shown in Fig. 9, have been verified by Ponyatovskij[16] who observed an overcooling of the bcc phase into fcc and hcp iron.

(4) The lines separating the phases in Fig. 10(a) are drawn from an insufficient number of experimental points[9] in order to illustrate conclusively our theoretical prediction that they should be straight lines. In contrast, the phase diagram of thallium, measured by Jajaraman *et al.*[10] in the vicinity of the triple point, clearly confirms this property. In Fig. 10(b) the experimental points given by these authors are superposed to be theoretical curves calculated for the transition and limit of stability lines. A linear transformation of the (a_1,b_1) plane into the pressure-temperature plane has been performed for comparison with experiment. One can verify in Fig. 10(b) that a very good fit is obtained between the theoretical lines and the experimental points.

In conclusion, let us stress that, in the framework of the model presented in this paper, the fcc-to-hcp transformation is interpreted as a displacive transition between two low-symmetry phases which are both derived from a common parent bcc structure. This interpretation is at variance with the one recently proposed by us[4] for the fcc-hcp transformation in Co and ^{4}He. The experimental data available for crystals of the elements[6,13] actually reveals that two classes of fcc-hcp transitions should be distinguished.

(1) A first class pertains to the fcc-hcp transition in ^{4}He, ^{3}He, Co, Pb, La, Ce, Pr, Nd, Sm, and Am. Here, only one of the two phases (fcc or hcp) is adjacent to the bcc phase (at least when this latter phase is found in the phase diagram). In this case, as shown in Ref. 3, one can interpret the fcc-hcp transformation by a reordering mechanism, the parent phase being formed by an hexagonal disordered polytype structure, as it is observed, for example, in cobalt.[17]

(2) A second class contains the elements, namely Fe, Tl, Ba, and Yb for which the two fcc and hcp phases have a region of coexistence with the bcc phase. For this case, which has been discussed in the present paper, two independent displacive mechanisms from the bcc structure provide a coherent interpretation of the entire phase diagram.

Although the distinction between the two preceding classes of fcc-hcp transformations may appear as arbitrary, one must keep in mind that, when dealing with strongly first-order transformations, one cannot discriminate a displacive or reordering mechanism *at* or *below* the transition, since, in both cases, a jump of the atoms takes place discontinuously from one equilibrium position to the other. In contrast, one can distinguish which of the two mechanisms is involved by considering the dynamical effects observed *above* the transition, i.e., in the parent phase.

[1]V. P. Dmitriev, S. B. Rochal, Yu. M. Gufan, and P. Tolédano, Phys, Rev. Lett. **60**, 1958 (1988).

[2]Yu. M. Gufan, V. P. Dmitriev, and P. Tolédano, Fiz. Tverd. Tela (Leningrad) **30**, 1057 (1988) [Sov. Phys. Solid State **30**, 613 (1988)].

[3]V. P. Dmitriev, S. B. Rochal, Yu. M. Gufan, and P. Tolédano, Phys. Rev. Lett. **62**, 844 (1989).

[4]V. P. Dmitriev, S. B. Rochal, Yu. M. Gufan, and P. Tolédano, Phys. Rev. Lett. **62**, 2495 (1989).

[5]V. P. Dmitriev, S. B. Rochal, Yu. M. Gufan, and P. Tolédano,

Ferroelectrics **79**, 11 (1988).
[6]J. Donohue, *The Structure of the Elements* (Wiley, New York, 1974).
[7]W. G. Burgers, Physica **1**, 561 (1934).
[8]E. C. Bain, Trans. AIME **70**, 25 (1924).
[9]E. Yu. Tonkov, *Phase Diagram of the Elements Under Pressure* (Nauka, Moscow, 1979), and references therein.
[10]A. Jajaraman, W. Klement, R. C. Newton, and G. C. Kennedy, J. Phys. Chem. Solids **24**, 7 (1963).
[11]O. V. Kovalev, *Irreducible Representations of the Space Groups* (Gordon and Breach, New York, 1965).
[12]J. C. Tolédano and P. Tolédano, Phys. Rev. B **21**, 1139 (1980).
[13]R. W. G. Wyckoff, *Crystal Structures* (Interscience, New York, 1960), Vol. 1.
[14]H. Warlimont and L. Delaey, *Martensitic Transformations in Copper-Silver and Gold Based Alloys* (Pergamon, Oxford, 1974), Chap. 3.
[15]J. C. Tolédano and P. Tolédano, *The Landau Theory of Phase Transitions* (World-Scientific, Singapore, 1978), Chap. 3.
[16]E. G. Ponyatovskij, Kristallografiya **4**, 257 (1959).
[17]O.S. Edwards and H. Lipson, Proc. R. Soc. (London), Ser. A **180**, 268 (1942).